Assessment of the Al–Fe–Ti system

M. Palm and J. Lacaze

Max-Planck-Institut für Eisenforschung GmbH, Max-Planck-Str. 1, D-40237 Düsseldorf, Germany
CIRIMAT-ENSIACET, F-31077 Toulouse, France

Abstract

The Al–Fe–Ti system has been assessed and the limiting binary systems are shortly reviewed. Based on a thorough review of the literature, isotherms at 800, 900, and 1000 °C have been re-evaluated and a provisional isotherm at 1200 °C is presented for the first time. The effect of alloying the binary phases with the third component is reviewed with regard to the ternary homogeneity ranges, crystallography, order/disorder transformations, and site occupancies. Of the variously reported ternary compounds only the existence of "Al_2FeTi" (τ_2) and "Al_8FeTi_3" (τ_3) is confirmed. The occurrence of the phases τ_2^*, τ'_2, and of a new stacking variant of TiAl is still under discussion, while the existence of the phases Fe_2AlTi (τ_1) and $Fe_{25}Al_{69}Ti_6$ (X) is ruled out. The presented reaction scheme corroborates the isothermal sections and also a representation of the liquidus surface is given. Magnetic, electrical, thermochemical, atomistic and diffusion data for Al–Fe–Ti alloys are summarised and an overview about studies on modelling of phase equilibria and phase transformations is given.

Keywords: A. Ternary alloy systems; B. Phase diagrams; B. Crystal chemistry of intermetallics; B. Crystallography; B. Order/disorder transformations

1. Introduction

Phase equilibria in the Al–Fe–Ti system are of considerable interest as Al–Fe–Ti-based alloys have been considered in connection with a variety of applications. Besides for medical applications [1] and [2] and in connection with grain refinement of Al-base materials [3], Al–Fe–Ti-based alloys are considered to have a considerable potential for the development of intermetallic-based materials for high-temperature applications [4] and [5]. Especially Fe–Al-based alloys are of interest in this respect and therefore their mechanical properties and oxidation behaviour have been studied in some detail [6], [7], [8], [9], [10], [11], [12], [13] and [14]. Also the mechanical behaviour of the $L1_2$-ordered phase τ_3 [15], [16] and [17] and of the ternary Laves phase [18] has been investigated. During recent efforts to develop TiAl-base alloys for structural applications only little information has been gained on the effect of Fe additions on mechanical properties [19]. Because joining with Fe-base materials, e.g. steels, is vital for the application of TiAl-base materials, the phases occurring along the TiAl–Fe diffusion path have been studied [20]. Also a patent for an oxidation-resistant Ti–Al–Fe alloy for use as diffusion barrier coating has been granted [21].

Compared to other ternary systems the Al–Fe–Ti system has been very well investigated and these data have been compiled and assessed before. The assessment of the Al–Fe–Ti system by Raghavan [22] has been updated twice since then [23] and [24]. Descriptions of the Al–Fe–Ti system have also been presented by Kumar [25] and in the relevant compendia on ternary alloy systems [26] and [27]. The current assessment presents a critical re-evaluation and update of these data.

2. Binary sub-systems

2.1. Fe–Ti system

The Fe–Ti system is discussed in detail in the accompanying paper on the Fe–Ni–Ti system and therefore the reader is referred to that paper for the discussion of the Fe–Ti phase diagram. For the isothermal sections shown in the present paper the data from the assessment of Murray [28] have been taken.

2.2. Al–Ti system

Following the elaborate assessment by Murray [29] the Al–Ti system has been updated regularly [30], [31] and [32]. Only recently a new comprehensive assessment of the Al–Ti phase diagram has been performed [33] and the reader is referred to that publication for any details. The phase diagram derived from this assessment is shown in Fig. 1. Compared to the latest update of the Al–Ti phase diagram [32] it differs especially in the Al-rich part, as the assessment takes into account results from a number of recent papers, which have not yet been covered in the update. It is noted that none of the CALPHAD-type descriptions based on the available thermodynamic data [34], [35], [36], [37], [38], [39], [40], [41], [42], [43], [44], [45], [46] and [47] matches the assessed phase diagram as a whole, though remarkable agreements between individual equilibria of the assessed phase diagram and the calculated ones exist.

Fig. 1. The Al–Ti system according to the most recent assessment [33].

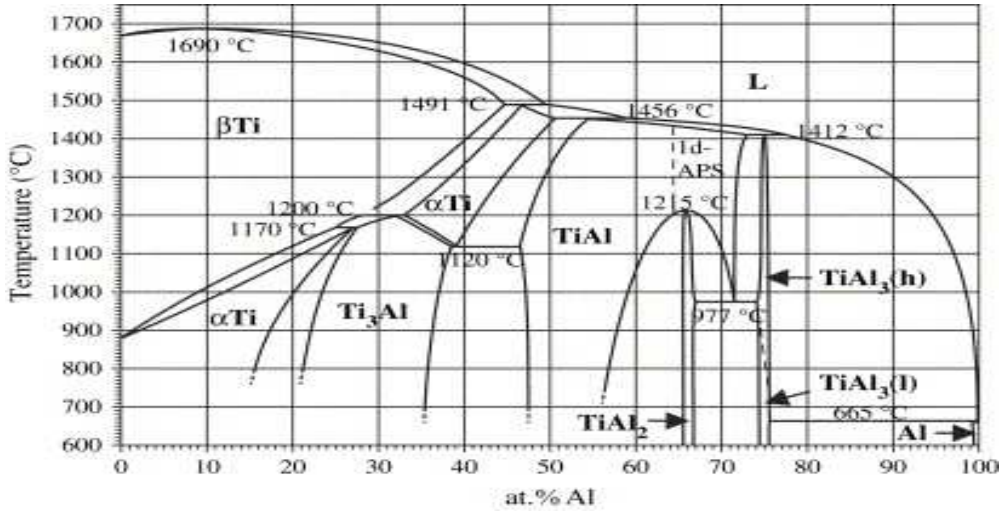

2.3. Al–Fe system

Since the assessment of the Fe–Al system by Kattner [48] (Fig. 2) numerous new results have been obtained within this system. Many of them concern details of the B2 and $D0_3$ orderings and the variation of the vacancy concentration as function of temperature and composition in the Fe-rich part of the system. As they are too numerous to be dealt with in detail within the scope of the present assessment, discussion will focus on selected works only.

Fig. 2. The Fe–Al system according to the assessment by Kattner [48].

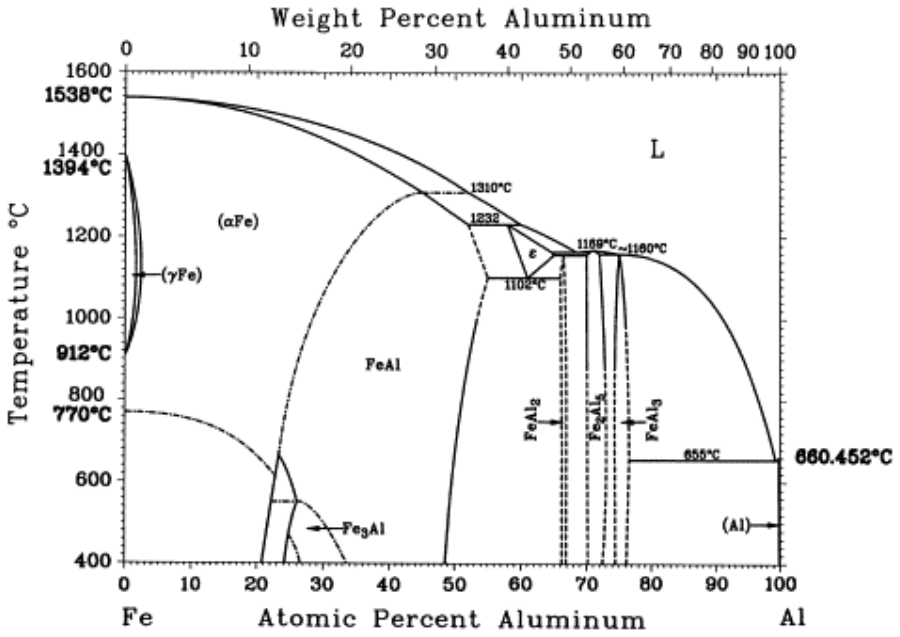

The phase equilibria between αFe (A2), FeAl (B2), and Fe_3Al ($D0_3$) have been re-investigated by in situ high-temperature neutron diffraction [49] and by investigations of diffusion couples [50]. In the latter study it was found that the αFe/αFe + Fe_3Al phase boundary is actually at higher Fe contents below 450 °C than suggested in the assessment by Kattner [48]. The phase equilibria between the bcc phases have also been calculated by the Monte Carlo (MC) method [51], MC and cluster variation (CVM) methods [52], and the Kirkwood method [53]. Compositions of the Al-rich intermetallic phases at 1000 °C have been experimentally determined in Refs. [54] and [55].

The liquidus in the Al-rich part has been investigated by differential thermal analysis (DTA) [56]. It has also been investigated by differential scanning calorimetry (DSC) and subsequently the stable and metastable Al-rich parts have been calculated [57]. The solubility of Fe in liquid Al has been calculated by Pashechko and Vasyliv [58].

Data for the crystallographic structures of Fe_2Al_5 [59] and [60] and Fe_4Al_{13} ($FeAl_3$) [61] and [62] have been published. The crystallographic structure of the high-temperature phase is still not settled [63] as this phase decomposes spontaneously during quenching. Results from ternary Fe–Al–X alloys indicate that it may have the hexagonal Al_8Cr_5-type structure [64], [65] and [66].

3. Effect of alloying the binary phases with the third component

A prominent feature of the Al–Fe–Ti system is the large solid solubility of Al in the binary Fe–Ti phases. In the C14-type Laves phase Fe_2Ti (crystallographic data of all phases are given in Table 1) more than two-thirds of Fe can be substituted by Al [67]. Al substitutes for Fe on both of the two different crystallographic Fe positions alike and no transformation to another Laves phase polytype has been reported. The substitution of Fe by Al leads to an increase in the lattice parameters and their dependence on composition has been determined [67] and [68].

Table 1.

Crystallographic structures of the binary compounds

Phase	Pearson symbol	Space group	Strukturbericht designation	Prototype	Solid solubility of the third component (at.%)	Lattice parameter(s) (nm)	Temperature (°C)	Reference
Fe_2Ti (λ)	hP12	$P6_3/mmc$	C14	$MgZn_2$	47.0 Al	a_0 = 0.5038(1)	1000	[67]
						c_0 = 0.8193(1)		
FeTi	cP2	$Pm\bar{3}m$	B2	CsCl	42 Al	a_0 = 0.3175	1300	[69]
βTi	cI2	$Im\bar{3}m$	A2	W	~25 Al	n.d.	1000	[71]

Phase	Pearson symbol	Space group	Strukturbericht designation	Prototype	Solid solubility of the third component (at.%)	Lattice parameter(s) (nm)	Temperature (°C)	Reference
						(a_0 = 0.31617(8) for $Fe_{15.1}Al_{22.1}Ti_{62.8}$)		
αTi	hP2	$P6_3/mmc$	A3	Mg	1.2 Fe	n.d.	1300	[72]
Ti_3Al (α_2)	hP8	$P6_3/mmc$	Ni_3Sn	$D0_{19}$	1.5 Fe	a_0 = 0.5772(1)	800	[67]
						c_0 = 0.46324(9) for $Fe_{1.5}Al_{30.8}Ti_{67.7}$		
TiAl (γ)	tP4	$P4/mmm$	$L1_0$	AuCu	2.6 Fe	a_0 = 0.3999(1)	800	[67]
						c_0 = 0.4072(2) for $Fe_{2.6}Al_{46.1}Ti_{51.3}$		
$TiAl_2$	tI24	$I4_1/amd$	–	$HfGa_2$	2.5 Fe	a_0 = 0.3966(2)	800 and 1000	[67]
						c_0 = 2.431(2) for $Fe_{2.4}Al_{63.7}Ti_{33.9}$		
$TiAl_3$ (h)	tI8	$I4/mmm$	$D0_{22}$	$TiAl_3$ (h)	1.2 Fe	a_0 = 0.3847(1)	800	[67]
						c_0 = 0.8602(5)		
$TiAl_3$ (l) (Ti_8Al_{24})	tI32	$I4/mmm$	–	$TiAl_3$ (l)	n.d.			
γFe	cF4	$Fm\bar{3}m$	A1	Cu	n.d.			
αFe	cI2	$Im\bar{3}m$	A2	W	9.2 Ti	n.d.	1000	[67]
FeAl (α_2)	cP2	$Pm\bar{3}m$	B2	CsCl	10.6 Ti	a_0 = 0.29252(8) for $Fe_{49.7}Al_{39.7}Ti_{10.6}$	1000	[67]
Fe_3Al	cF16	$Fm\bar{3}m$	$D0_3$	BiF_3	25.0 Ti	a_0 = 0.58780	1000	[67]

Phase	Pearson symbol	Space group	Strukturbericht designation	Prototype	Solid solubility of the third component (at.%)	Lattice parameter(s) (nm)	Temperature (°C)	Reference
						(6)		
ε	(hR26)	(*R*3*m*)	($D8_{10}$)	(Al_8Cr_5)	6.5 Ti	a_0 = 1.268(4)	>1100	[66]
						b_0 = 0.790(3)		
$FeAl_2$	aP18	*P*1	–	$FeAl_2$	1.8 Ti	a_0 = 0.4872(2))	1000	[67]
						b_0 = 0.6459(2)		
						c_0 = 0.8794(4)		
						α = 91.76(3)		
						β = 73.35(3)		
						γ = 96.89(3		
Fe_2Al_5	oC*	*Cmcm*	–	Fe_2Al_5	2.5 Ti	a_0 = 0.7656(2)	1000	[67]
						b_0 = 0.6463(4)		
						c_0 = 0.4229(2)		
Fe_4Al_{13}($FeAl_3$)	mC102	*C*2/*m*	–	Fe_4Al_{13}	6.5 Ti	n.d.	800	[67]

The maximum solid solubility for the third component, the lattice parameter(s) for this composition, the temperature for the maximum solid solubility and the respective reference are given. The structure of ε is tentative (see text) and their description is therefore given in brackets. n.d.: not determined.

In B2-ordered FeTi Al can also substitute for Fe to a large extent. At 1300 °C a composition of $Fe_5Al_{42}Ti_{53}$ has been reported [69] (all compositions are given in at.% throughout this paper). Apparently the B2 order is not affected by this substitution. The dependence of the lattice constant on composition has been determined in Refs. [67] and [70]. In both phases,

Fe_2Ti and FeTi, the solid solubility for Al increases markedly with increasing temperature [67].

Disordered βTi (A2) as well has a marked solid solubility for Al of about 25 at.% [71]. Kainuma et al. [71] found that βTi becomes ordered B2 by progressive substitution of Ti by Fe + Al. At 1000 °C they found a continuous range of solid solutions between βTi (A2) and FeTi (B2) with a second order disorder–order transition from A2 to B2 at about 70 at.% Ti. Though, the course of the tie-lines on the Ti-side in Ref. [71] suggests the existence of a three-phase field A2 + B2 + Ti_3Al at this temperature, i.e. the existence of a first-order transition with a narrow A2 + B2 two-phase field. Nevertheless the A2/B2 transition may change from first to second order at somewhat higher temperatures.

The solid solubility for Fe in all Al–Ti phases is very limited. The maximum content of Fe in αTi is about 1 at.% at an Al content of 44 at.% [72]. For more Ti-rich compositions the solid solubility for Fe in αTi is even more restricted. For Ti_3Al, TiAl, $TiAl_2$ and $TiAl_3$ the solid solubility for Fe ranges between 1.2 and 2.5 at.% [67] and [73] and varies little with temperature [67] (cf. Table 1). The site occupancies in TiAl and Ti_3Al alloyed with Fe have been experimentally determined by atom location channelling enhanced microanalysis (ALCHEMI) [74].

γFe has only a very limited solid solubility for both Al and Ti. The solid solubility for Ti in αFe (A2) and FeAl (B2) increases with increasing temperature and both phases contain up to about 10 at.% Ti at 1000 °C [67]. The site occupancy of Ti in B2-ordered FeAl has been determined by ALCHEMI [75] and has been modeled [76] and [77]. $D0_3$-ordered Fe_3Al can even contain up to 25 at.% Ti in solid solution [67] and [78].

By alloying Fe-rich Fe–Al alloys with Ti the transition temperatures for the $D0_3$/B2 and B2/A2 transitions increase markedly [8], [13], [78], [79], [80], [81], [82], [83] and [84]. The $D0_3$-type ordering is maintained because Ti substitutes in Fe_3Al for Fe on ½ ½ ½, the 4(b) Wyckoff site of the lattice [85] and [86]. Ohnuma et al. [78] studied in detail the dependence of the transition temperatures on composition. They found that the $D0_3$-structure is stable between binary Fe–25 at.%Al and Fe–25 at.%Al–25 at.%Ti and that the $D0_3$/B2 transition temperature simultaneously increases from 547 °C in the binary to 1212 °C in the ternary system. No clear distinction has been made up to now when this phase is denoted as $D0_3$ (binary) or $L2_1$ (ternary, Heusler-type). The lattice parameter of $D0_3$ increases by the

substitution of Fe by Ti and its dependence on composition has been determined in Refs. [84] and [87]. An increase of the lattice parameter was also observed with increasing Ti content along $FeAl_{(1-x)}Ti_x$ [88].

Because the binary compound ▫decomposes by a eutectoid reaction during quenching to room temperature its crystallographic structure has not been determined yet. Also as-cast ternary Al–Fe–Ti alloys with compositions near this binary phase show similar fine-scaled microstructures, which presumably were generated by eutectoid decomposition of ▫during cooling [66]. EDS analyses of some unaltered grains revealed that they contained at least 6.5 at.% Ti. XRD indicates that these grains have the hexagonal Al_8Cr_5-type structure and provisional lattice constants have been established as a_0 = 1.268(4) nm and c_0 = 0.790(3) nm [66]. It is assumed that this is not a ternary phase but that this composition lies within the ternary solid solubility range of the binary phase ▫.

$FeAl_2$ and Fe_2Al_5 both have limited solid solubilities for Ti of 1.8 and 2.5 at.%, respectively [67]. Fe_4Al_{13} can dissolve about 6.5 at.% Ti [67]. A structure refinement of Fe_4Al_{13} containing about 5.5 at.% Ti revealed that Ti replaces Al only on certain crystallographic sites [89].

4. Ternary phases

The existence of two ternary intermetallic phases has been confirmed. The phase τ_2 is stable over a wide range of compositions and, depending on composition, exists in two polytypes [67]. Between $Fe_{24.5}Al_{24.6}Ti_{50.9}$ and $Fe_{21.4}Al_{47.8}Ti_{30.8}$ the phase has a complex fcc structure ($Mn_{23}Th_6$ type; cf. Table 2), while at lower Ti contents, i.e. from $Fe_{27.0}Al_{49.0}Ti_{24.0}$ to $Fe_{25.1}Al_{53.6}Ti_{21.3}$, the phase is primitive tetragonal (τ_2^*). The Ti-rich polytype forms on cooling by the peritectoid reaction TiAl + FeTi + $Fe_2Ti \leftrightarrow \tau_2$ (Pd_1) at about 1075 °C while the Al-rich polytype forms by the peritectic reaction L + τ_3 + $Fe_2Ti \leftrightarrow \tau_2^*$ (P_2) at about 1225 °C [66]. Whether these two polytypes correspond to those two structural variants of τ_2 found in the Al–Co–Ti system [90] has to be settled. Preliminary results of a detailed investigation on the stability of the τ_2^* polytype in the Al–Fe–Ti system have confirmed the presence of τ_2^* in quenched samples, but first results of in situ neutron diffraction experiments failed to prove the existence of the tetragonally distorted τ_2^* polytype at 800 °C, where instead the cubic τ_2 polytype was found [91].

Table 2.

Crystallographic structures of the ternary Al–Fe–Ti compounds

Phase	Pearson symbol	Space group	Strukturbericht designation	Prototype	Solid solubility range (at.%)	Lattice parameters (nm)	Reference
"Al_2FeTi" (τ_2)	cF116	$Fm\bar{3}m$	$D8_a$	$Mn_{23}Th_6$	$Fe_{24.5}Al_{24.6}Ti_{50.9}$	a_0 = 1.2110(3)	[67]
					$Fe_{21.4}Al_{47.8}Ti_{30.8}$	a_0 = 1.2038(2)	
τ_2*	tP*				$Fe_{27.0}Al_{49.0}Ti_{24.0}$	a_0 = 1.1973(1)	[67]
						c_0 = 1.27683(3)	
					$Fe_{25.1}Al_{53.6}Ti_{21.3}$	a_0 = 1.19590(5)	
						a_0 = 1.2746(1)	
"Al_8FeTi_3" (τ_3)	cP4	$Pm\bar{3}m$	$L1_2$	$AuCu_3$	$Fe_{7.5}Al_{63.9}Ti_{28.6}$	a_0 = 0.3943(1)	[67]
					$Fe_{7.6}Al_{66.6}Ti_{25.8}$	a_0 = 0.39444(5)	

The cubic phase τ_3 with $L1_2$ structure is stable at compositions of 7.5 at.% Fe, 63.9–66.6 at.% Al and 28.6–25.8 at.% Ti, and no marked broadening of the single-phase field is observed with temperature between 800 and 1000 °C [67]. Data available for 1200 °C indicate that at this temperature τ_3 is stable within a wider range of compositions [92]. Site preferences in τ_3 and the long-range order parameter have been determined in Refs. [16], [93] and [94].

The existence of the phases Fe_2AlTi (τ_1, Heusler-type phase with $L2_1$ structure [95]) and $Fe_{25}Al_{69}Ti_6$ (X, "low symmetry" [68]) has to be ruled out [22]. Both phases are apparently no phases on their own. While τ_1 corresponds to the maximum solid solubility of Ti in Fe_3Al, $Fe_{25}Al_{69}Ti_6$ most likely has been confused with the extended homogeneity range of Fe_4Al_{13}.

Three more phases have been described recently, though not enough details are known right now to decide whether these are stable ternary phases. Two of these phases actually may not be true ternary compounds, but may form continuous solid solutions with binary compounds. This point has not been settled because the individual homogeneity ranges of the phases in question have not been established yet as function of temperature and composition.

At a composition of 60.5 Al, 33.0 Fe, 6.5 Ti Ducher et al. [66] detected a hexagonal phase of Al_8C_5 type. It is assumed that this is actually not a ternary phase, but represents the ternary solid solubility range of ε (see also above).

Ducher et al. [96] found extra diffraction spots in TiAl that has been alloyed with Fe. The diffraction pattern could be explained in that by adding Fe the stacking sequence in $\{111\}_{L10}$ is modified. Though the original description of this phase actually came from a quinary alloy, the same type of ordering was later on found in an as-cast ternary alloy at a composition of 46.5 at.% Al, 2.5 at.% Fe, 51.0 at.% Ti [20]. Whether this is a stable phase and if it forms continuously from TiAl or if it is separated from TiAl by a two-phase field has not been established yet.

Levin et al. [69], [97], [98] and [99] studied the evolution of the microstructure in an alloy containing 48.5 at.% Al, 1.9 at.% Fe, 49.6 at.% Ti after various heat treatments. At a composition of 38 at.% Al, 10 at.% Fe and 52 at.% Ti they observed a phase with a tetragonal unit cell of a_0 = 1.15 nm, c_0 = 1.38 nm. The phase was found in samples which were water-quenched after annealing at 1400 and 1200 °C [69] and [98], but not in samples which were slowly cooled from this temperatures or water-quenched from 700 to 1070 °C [99]. The phase has been denoted as τ'_2, as it had been originally considered to be the tetragonal polytype of the τ_2 phase [69]. Subsequent investigations revealed that τ'_2 forms during cooling from Al-rich B2-ordered FeTi [98]. That τ'_2 may be a metastable phase is indicated by the fact that the compositions of the other phases measured in a τ'_2-containing sample that has been water-quenched from 1200 °C [98] differ from those reported by Kainuma et al. [72] for the same composition range. Still details on the stability of the three phases discussed above need further clarification.

5. Liquidus surface

The basic layout of the liquidus surface has been established by Seibold [95] and though further amendments have been made [22] and [24] even the latest of these versions had been considered as tentative. Therefore, Ducher et al. re-investigated the liquidus surface by DTA and by performing optical microscopy, X-ray diffraction (XRD), and energy dispersive analyses on a scanning electron microscope (SEM–EDS) on as-cast samples [66]. The liquidus projection shown in Fig. 3 is based on that study. Compared to the last – tentative – version by Raghavan [24] it differs mainly in that there is no primary field of solidification of

the Ti-rich polytype of τ_2 and no continuous solid solubility between βTi and FeTi exists up to the liquidus. Actually, τ_2 was found to decompose at 1075 °C by the peritectoid reaction: TiAl + FeTi + $Fe_2Ti \leftrightarrow \tau_2$ (Ti-rich) (Pd_1) as mentioned above. Otherwise there are some changes regarding the positions of invariant lines. Most prominent is the finding that the area of primary solidification of ε extends up to the eutectic trough.

Fig. 3. Liquidus projection of the Al–Fe–Ti system based on Ref. [66]. Dots correspond to alloys for which the indicated liquidus temperatures (in °C) have been determined by DTA. Single and double arrows designate peritectic and eutectic reactions, respectively. Invariant reactions are labelled according to the reaction scheme shown in Fig. 4. Isotherms are tentative.

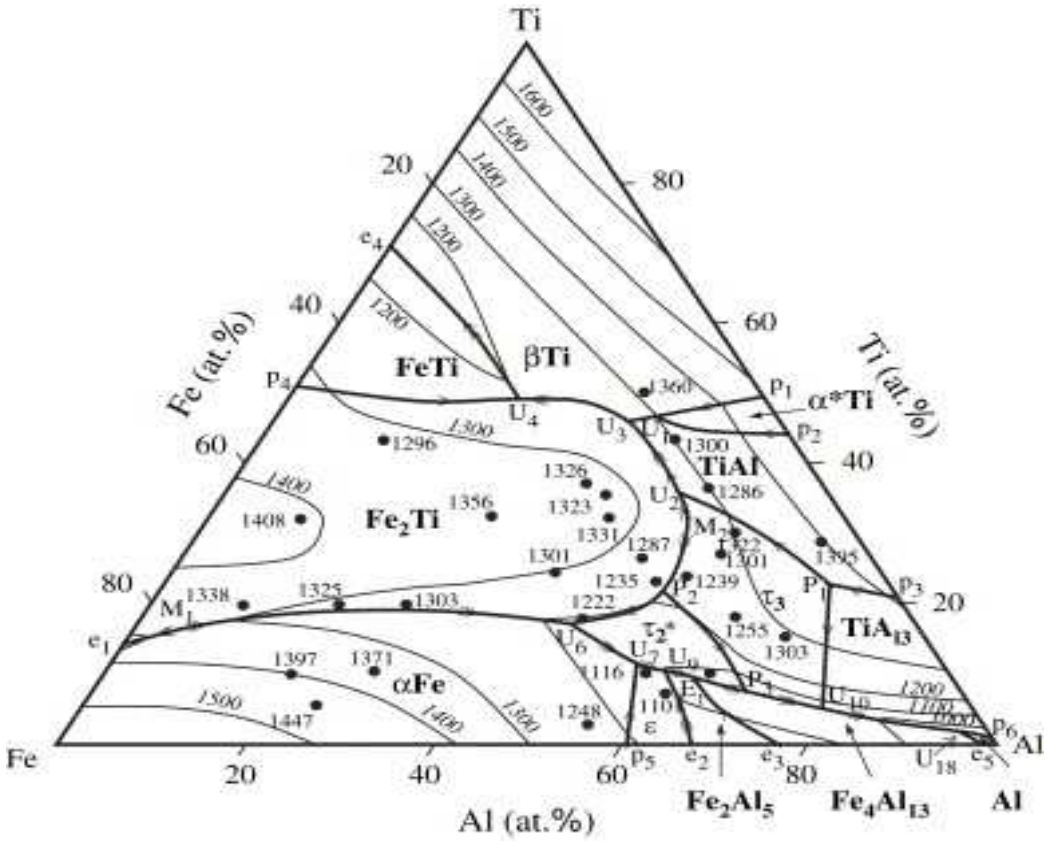

6. Invariant reactions and reaction scheme

Reaction schemes of the Al–Fe–Ti system have been previously presented [22], [24], [26], [66], [67] and [95] and a discussion on various sections of the reaction scheme has been

provided by Ducher [20]. The reaction scheme shown in Fig. 4 is based on the recent one by Ducher et al. [66]. Amendments have been made in that data for invariant reactions in the Al–Ti system have been updated from Ref. [33]. From this update it is clear that the phase Al_5Ti_2 does not exist as such, but is a part of a series of one-dimensional antiphase domain structures (1d-APS). It is now confirmed that these structures are not separated from TiAl by a two-phase field above 1215 °C [100], [101] and [102], which implicates that they form either stably at high temperatures or metastably during cooling from Al-rich TiAl by ordering of excess aluminium. To take these new findings into account, the reactions "TiAl" ↔ TiAl + Ti_2Al_5 (c_1) and TiAl + Ti_2Al_5 ↔ $TiAl_2$ + τ_3 (U_5) from Ref. [66] have been replaced by TiAl/1d-APS ↔ $TiAl_2$ (c_1) and TiAl/1d-APS ↔ $TiAl_2$ + τ_3 (C_1), respectively, and the reaction TiAl + Ti_2Al_5 ↔ $TiAl_2$ (pd_1) at 1215 °C has been removed. Also some errors have been corrected. The peritectic reaction L + τ_2^* + τ_3 ↔ Fe_4Al_{13} at ≈1100 °C is now correctly denoted as P_3 (instead of E_3), the non-existing reaction L + τ_3 ↔ Fe_2Al_5 + τ_2^* (U_{10}) has been removed and the temperature for L + τ_3 ↔ $TiAl_3$ + Fe_4Al_{13} has been changed to ≈1070 °C [20].

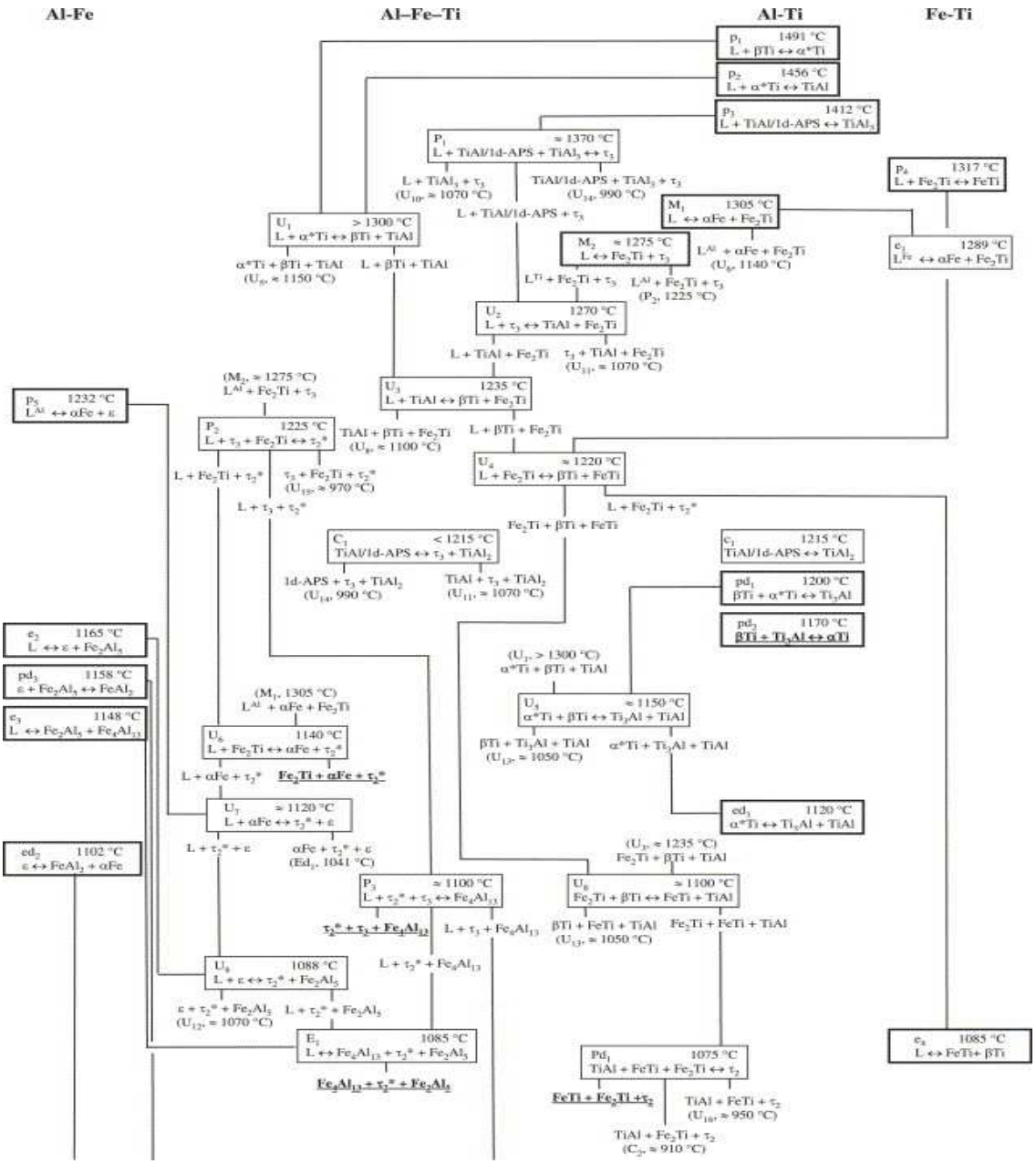
Al-Fe
Al–Fe–Ti
Al-Ti
Fe-Ti
p1 1491 °C
L + βTi ↔ α*Ti
p2 1456 °C
L + α*Ti ↔ TiAl
p3 1412 °C
L + TiAl/1d-APS ↔ TiAl3
P1 ≈ 1370 °C
L + TiAl/1d-APS + TiAl3 ↔ τ3
L + TiAl3 + τ3 (U10, ≈ 1070 °C)
TiAl/1d-APS + TiAl3 + τ3 (U14, 990 °C)
L + TiAl/1d-APS + τ3
p4 1317 °C
L + Fe2Ti ↔ FeTi
M1 1305 °C
L ↔ αFe + Fe2Ti
U1 > 1300 °C
L + α*Ti ↔ βTi + TiAl
M2 ≈ 1275 °C
L ↔ Fe2Ti + τ3
LAl + αFe + Fe2Ti (U8, 1140 °C)
e1 1289 °C
LFe ↔ αFe + Fe2Ti
α*Ti + βTi + TiAl (U9, ≈ 1150 °C)
L + βTi + TiAl
LTi + Fe2Ti + τ3
LAl + Fe2Ti + τ3 (P2, 1225 °C)
U2 1270 °C
L + τ3 ↔ TiAl + Fe2Ti
L + TiAl + Fe2Ti
τ3 + TiAl + Fe2Ti (U11, ≈ 1070 °C)
(M2, ≈ 1275 °C)
LAl + Fe2Ti + τ3
P5 1232 °C
LAl ↔ αFe + ε
U3 1235 °C
L + TiAl ↔ βTi + Fe2Ti
P2 1225 °C
L + τ3 + Fe2Ti ↔ τ2*
TiAl + βTi + Fe2Ti (U8, ≈ 1100 °C)
L + βTi + Fe2Ti
L + Fe2Ti + τ2*
τ3 + Fe2Ti + τ2* (U13, ≈ 970 °C)
U4 ≈ 1220 °C
L + Fe2Ti ↔ βTi + FeTi
L + τ3 + τ2*
L + Fe2Ti + τ2*
Fe2Ti + βTi + FeTi
C1 < 1215 °C
TiAl/1d-APS ↔ τ3 + TiAl2
c1 1215 °C
TiAl/1d-APS ↔ TiAl2
1d-APS + τ3 + TiAl2 (U14, 990 °C)
TiAl + τ3 + TiAl2 (U11, ≈ 1070 °C)
pd1 1200 °C
βTi + α*Ti ↔ Ti3Al
pd2 1170 °C
βTi + Ti3Al ↔ αTi
e2 1165 °C
L ↔ ε + Fe2Al5
pd3 1158 °C
ε + Fe2Al5 ↔ FeAl2
e3 1148 °C
L ↔ Fe2Al5 + Fe4Al13
(M1, 1305 °C)
LAl + αFe + Fe2Ti
U6 1140 °C
L + Fe2Ti ↔ αFe + τ2*
L + αFe + τ2*
Fe2Ti + αFe + τ2*
(U7, > 1300 °C)
α*Ti + βTi + TiAl
U5 ≈ 1150 °C
α*Ti + βTi ↔ Ti3Al + TiAl
βTi + Ti3Al + TiAl (U13, ≈ 1050 °C)
α*Ti + Ti3Al + TiAl
ed3 1120 °C
α*Ti ↔ Ti3Al + TiAl
U7 ≈ 1120 °C
L + αFe ↔ τ2* + ε
ed2 1102 °C
ε ↔ FeAl2 + αFe
L + τ2* + ε
αFe + τ2* + ε (Ed3, 1041 °C)
(U7, ≈ 1235 °C)
Fe2Ti + βTi + TiAl
P3 ≈ 1100 °C
L + τ2* + τ3 ↔ Fe4Al13
U8 ≈ 1100 °C
Fe2Ti + βTi ↔ FeTi + TiAl
τ2* + τ3 + Fe4Al13
L + τ3 + Fe6Al13
βTi + FeTi + TiAl (U13, ≈ 1050 °C)
Fe2Ti + FeTi + TiAl
U9 1088 °C
L + ε ↔ τ2* + Fe2Al5
L + τ2* + Fe6Al13
ε + τ2* + Fe2Al5 (U12, ≈ 1070 °C)
L + τ2* + Fe2Al5
E1 1085 °C
L ↔ Fe6Al13 + τ2* + Fe2Al5
Fe6Al13 + τ2* + Fe2Al5
Pd1 1075 °C
TiAl + FeTi + Fe2Ti ↔ τ2
e4 1085 °C
L ↔ FeTi + βTi
FeTi + Fe2Ti + τ2
TiAl + FeTi + τ2 (U16, ≈ 950 °C)
TiAl + Fe2Ti + τ2 (C2, ≈ 910 °C)

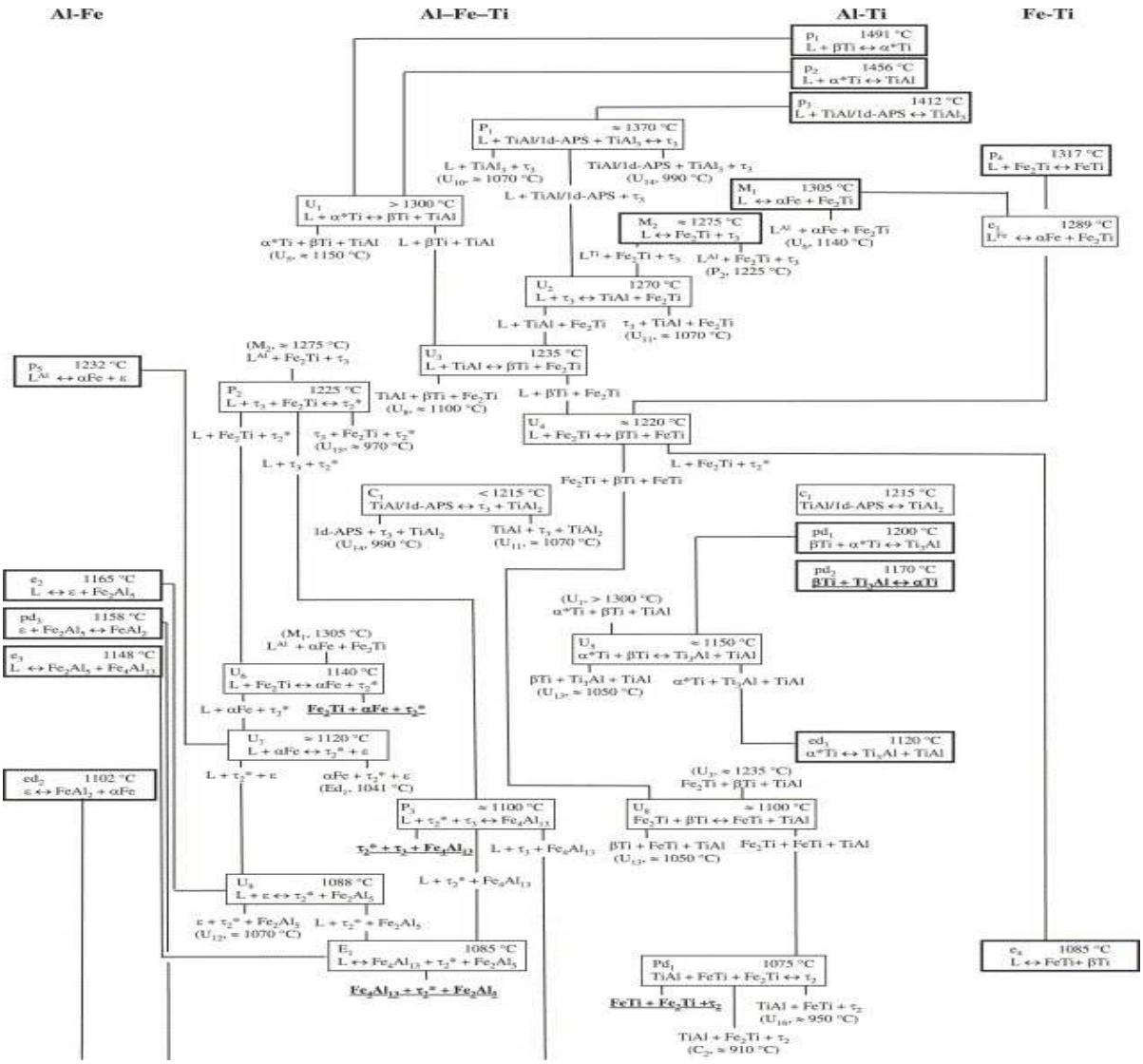

Fig. 4. Reaction scheme of the Al–Fe–Ti system. The scheme is based on the one by Ducher et al. [66]. Data for invariant reactions in the Al–Ti system have been updated from Schuster and Palm [33]. The following designations for the phases are used: τ_2, Ti-rich variant; τ_2^* Al-rich variant; αTi, low temperature (<1170 °C); α^*Ti, high temperature (>1120 °C); $L^{Al/Fe}$: two separate melts which exist below M_1. The different types of ordering in αFe (A2, B2, $D0_3/L2_1$), distinction between $TiAl_3$ (h) and $TiAl_3$ (l), and the possible merging of the phases FeTi and βTi at high temperatures are not taken into account (see text). Reactions are labelled as e/E: eutectic, p/P: peritectic, ed/Ed: eutectoid, pd/Pd: peritectoid, c/C: congruent, U: transition, M: maximum with small and capital letters denoting binary and ternary reactions, respectively. Bold boxes denote terminal reactions. Bold and underlined three-phase

equilibria are present in the isothermal section at 800 °C, the lowest temperature for which a complete isotherm exists.

It is noted that temperatures given for most solid-state reactions above 1000 °C are estimates, which need further study to be accurately established [66]. Ternary invariant reactions, for which temperatures have been established, e.g. by DTA, are TiAl + FeTi + $Fe_2Ti \leftrightarrow \tau_2$ (Pd_1) at 1075 °C [66], $\varepsilon \leftrightarrow \alpha Fe + FeAl_2 + \tau_2^*$ (Ed_1) at 1041 °C [66], and L + $TiAl_3 \leftrightarrow FeAl_3$ + Al at 658 °C (U_{18}) [103].

In the reaction scheme in Fig. 4 the different types of ordering in αFe (A2, B2, $D0_3/L2_1$) have not been taken into account. Also no distinction between $TiAl_3$ (h) and $TiAl_3$ (l) is made, as the details of the stability ranges of the two polymorphs have not been yet sufficiently established [33]. FeTi (B2) and βTi (A2) are treated as separate phases, though the two single-phase fields may merge at high temperatures [71].

The reaction scheme presented in Fig. 4 is in accordance with the recent versions of the binary sub-systems, with the liquidus projection shown in Fig. 3 and the isothermal sections, which are discussed in the following section.

7. Isothermal sections

Complete isothermal sections have been determined experimentally for 800 °C [67], [68] and [95], 900 °C [19] and 1000 °C [4] and [67] and in addition a number of partial isotherms have been determined. Table 3 summarises the experimental studies of phase equilibria in the Al–Fe–Ti system.

Table 3.

Experimental studies of phase equilibria in the Al–Fe–Ti system

Temperature (°C)	Composition range (at.%)	Number of alloys (heat treatment(s))	Experimental techniques	Reference
550, 800, 1000, 1100	Ti corner >60 at.% Ti	30 alloys (500 °C/500 h; 800 °C/200 h; 1000 °C/100 h; 1100 °C/100 h)	LOM, XRD	[123]
550, 800, 1100	Ti corner >60 at.% Ti	About 80 alloys (550 °C/1000 h; 800 °C/200–400 h; 1100 °C/6–75 h)	LOM, XRD	[124]

Temperature (°C)	Composition range (at.%)	Number of alloys (heat treatment(s))	Experimental techniques	Reference
550	Ti corner >58 at.% Ti	About 76 alloys (550 °C/1000 h)	LOM, XRD	[125]
700, 800	Ti corner >80 at.% Ti (αTi + βTi)	7 alloys (700 °C/720 h; 800 °C/240 h)	LOM, SEM, (TEM), EPMA	[104]
800	Full isotherm	>100 alloys (800 °C/600–900 h)	LOM, XRD	[68]
23, 800	>50 at.% Ti at 23 °C. Full isotherm at "about" 800 °C	about 64 alloys (800 °C/192 h)	LOM, XRD	[95]
800	Al-rich Al–Ti alloys <10 at.% Fe	12 alloys (800 °C/≥240 h)	SEM, HR-TEM, (EPMA)	[105]
800, 900	A2 + $L2_1$, B2 + $L2_1$	5 alloys, 2 diffusion couples (900 °C) (800 °C/672 h; 900 °C/336 h)	SEM, TEM, EPMA, DSC	[78]
800, 1000	Full isotherms	64 alloys (800 °C/500 h; 1000 °C/100 h; 6 diffusion couples 1000 °C/500 h)	LOM, SEM, XRD, EPMA	[67]
900	Full isotherm	30 alloys (900 °C/500 h)	LOM, XRD, EPMA	[19]
900	Ti_3Al + TiAl + 1–3 at.% Fe	13 alloys (900 °C/240 h)	XRD	[73]
1000	(Full isotherm) supplement to Ref. [67]	10 alloys (1000 °C/96 h)	LOM, XRD, EPMA	[4]
1000	Emphasis on phase equilibria with FeTi	25 alloys (1000 °C/500 h)	LOM, XRD, EPMA	[70]
1000	Ti-rich part >50 at.% Ti	14 alloys (1000 °C/168 h; 2 diffusion couples 1000 °C/3 h)	LOM, TEM, EPMA	[71]
1000, 1200, 1300	Phase equilibria among αTi, βTi, TiAl, Ti_3Al	5 alloys (1000 °C/168–504 h; 1200 °C/168 h; 1300 °C/24 h)	LOM, EPMA	[72]
1000, 1150	Emphasis on phase equilibria with Al_8FeTi_3 ($L1_2$)	14 alloys (1000 °C/144 h; 1150 °C/48 h) 35 alloys (1000 °C/48 h; 1150 °C/24 h)	LOM, SEM, (TEM), XRD, EPMA	[107]
1200	Phase equilibria with Al_8FeTi_3 ($L1_2$)	9 alloys (1200 °C/500 h)	LOM, SEM, (TEM, XRD), EPMA	[92]

LOM: Light optical microscopy; SEM: Scanning electron microscopy; TEM: Transmission electron microscopy; XRD: Powder X-ray diffraction; EPMA: Electron probe microanalysis; DSC: Differential scanning calorimetry; when given in brackets the technique has been employed but no specific results are reported.

As there are a considerable number of investigations on phase equilibria in the temperature range 800–1000 °C, which are at least to most parts qualitatively in accordance with each other, complete isotherms for 800 °C (Fig. 5a), 900 °C (Fig. 6) and 1000 °C (Fig. 7a) have been established. They are consistent with each other and the reaction scheme shown in Fig. 4.

Fig. 5. (a) Isothermal section of the Al–Fe–Ti system at 800 °C. The isotherm is based on the one given in Ref. [67]. Phase equilibria in the Fe corner have been modified according to the results shown in Fig. 5b. Dotted lines denote second-order transitions and dots on the axis mark compositions of binary phases. (b) Partial isothermal section of the Fe corner of the Al–Fe–Ti system at 800 °C. Phase relations between αFe (A2), FeAl (B2), and $Fe_2(Fe,Ti)_1Al$ ($D0_3/L2_1$) have been examined by high-temperature XRD [80], TEM and EPMA [79], DTA [20] and [82], measurement of the resistivity as function of temperature [83], DSC, TEM, and EPMA [78], and TEM and DTA [13]. Solid lines denote first-order transitions while dotted lines denote second-order transitions. Dashed lines depict phase equilibria from Palm et al. [67].

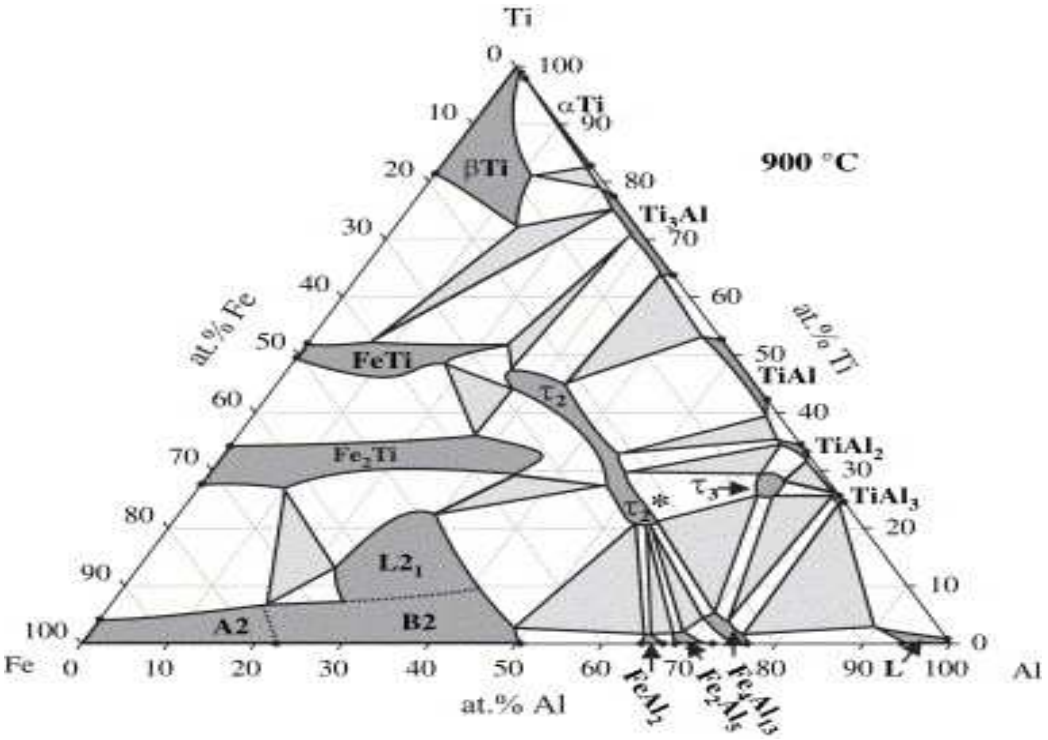

Fig. 6. Isothermal section of the Al–Fe–Ti system at 900 °C based on Ref. [106].

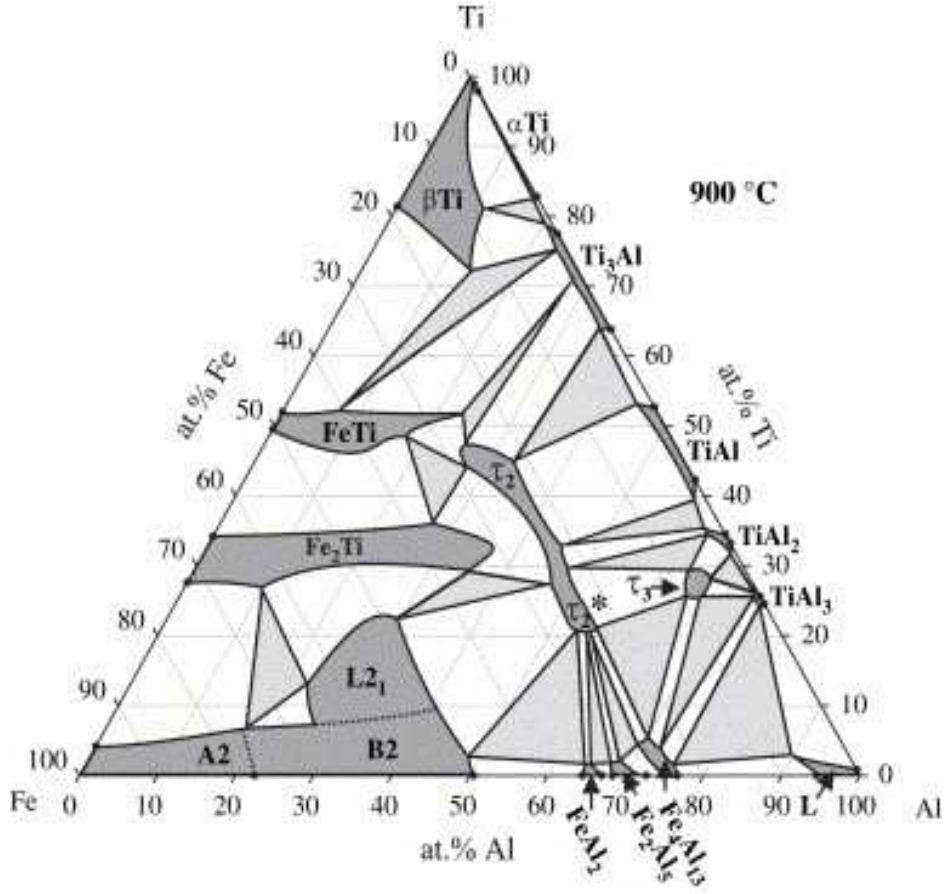

Fig. 7. (a) Isothermal section of the Al–Fe–Ti system at 1000 °C. Dotted lines denote second-order transitions and dots on the axis mark compositions of binary phases. (b) Partial isothermal section of the Fe corner of the Al–Fe–Ti system at 1000 °C. Phase equilibria among αFe (A2), FeAl (B2), and $Fe_2(Fe,Ti)_1Al$ ($D0_3/L2_1$) have been examined by TEM and EPMA [79], measurement of the resistivity as function of temperature [83], EPMA of diffusion couples [126], DSC, TEM, and EPMA [78], DTA [20], and TEM and DTA [13]. Additional EPMA results from Ref. [67] are given for the adjacent phase equilibria.

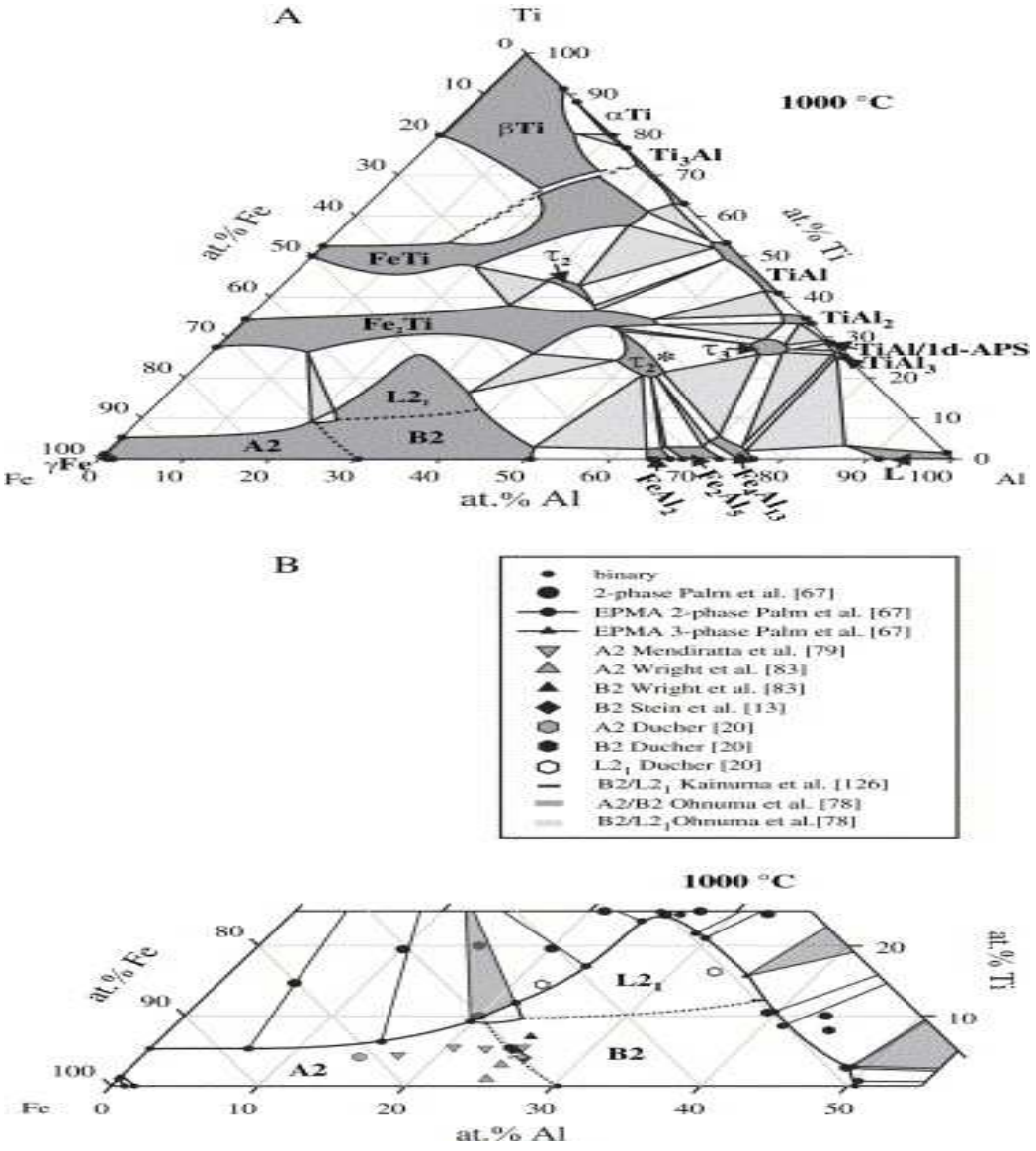

The isotherm for 800 °C (Fig. 5a) is based on the one by Palm et al. [67]. This isotherm had been experimentally determined by metallography, XRD, and EPMA on quenched samples (cf. Table 3). The common features and differences between this isotherm and previous investigations by Markiv et al. [68] and Seibold [95] have already been discussed [67]. Since then, few new data have become available. Nwobu et al. [104] determined the phase equilibria between αTi and βTi at 800 °C and their results are in good agreement with the isotherm shown in Fig. 5a. In contrast most of the data determined for Al-rich Al–Ti alloys with Fe contents up to 8 at.% Fe [105] are in disagreement with Fig. 5a. As these data apparently lead to the improbable phase diagram proposed by Yang and Goo [105] they have not been considered in Fig. 5a. Ohnuma et al. [78] investigated the ordering and phase separation in the

bcc phase in the Fe corner. Their results together with those of other studies [13], [20], [79], [80], [82] and [83] are shown in Fig. 5b. These results clearly show the existence of a two-phase field between αFe (A2) and $L2_1$, and the respective changes have been made in Fig. 5a. The isotherms shown in Figs. 5a, 6 and 7a have also been updated to comply with the recent assessment of the Al–Ti system [33].

Fig. 6 shows the isothermal section at 900 °C. It has been basically adopted from Ref. [106] with adjustments for the binary Fe–Ti and Al–Ti systems, the composition of the ternary melt [66], and the composition of FeTi at the three-phase equilibrium FeTi + Ti_3Al + τ_2. The only additional data which have become available at 900 °C since the previous study [106] are from Hao et al. [73] for the solid solubility of Fe in Ti_3Al and TiAl. Their data indicate a slightly higher solid solubility for Fe in these two phases than shown in Fig. 6 but are otherwise in full agreement with the phase equilibria shown in Fig. 6.

The isothermal section at 1000 °C (Fig. 7a) is based on the work by Gorzel et al. [4], which was an updated version of a previous study [67]. As for this temperature a considerable amount of additional data is available now, several amendments compared to the original isotherm have been made in Fig. 7a. Besides adjustments for the Fe–Ti and Al–Ti binary systems, the composition of the ternary melt has been corrected according to Ducher et al. [66]. Phase equilibria in the Ti-rich corner of the Al–Fe–Ti system at 1000 °C have been determined by Kainuma et al. [71]. Their compositions measured for two-phase FeTi + βTi fit perfectly with those from Palm et al. [67], while their other data supplement the missing phase equilibria in the Ti corner (Fig. 7a). Though Kainuma et al. found that βTi forms a continuous range of solid solutions with FeTi at 1000 °C this feature has not been adopted in Fig. 7a for reasons discussed in Section 3. Consequently the single-phase areas of βTi and FeTi as determined by Kainuma et al. [71] are separated by a narrow two-phase field in Fig. 7a and the adjacent three-phase equilibria are indicated by dashed lines. Mabuchi et al. [107] determined partial isothermal sections at 1000 and 1150 °C around the phase τ_3. Qualitatively most of their results for 1000 °C are in agreement with the isotherm shown in Fig. 7a, except that they find the two-phase equilibrium $TiAl_2$ + τ_2^* instead of Fe_2Ti + τ_3 at this temperature. As the respective invariant reaction involving these four phases takes place slightly below 1000 °C (U_{15} at ≈970 °C, Fig. 4) it is assumed that the blowing air quenching employed in Ref. [107] was insufficient to suppress this reaction on cooling. The stability ranges of A2, B2

and $D0_3/L2_1$ shown by dotted lines in Fig. 7a are derived from the summary of the experimental information in the Fe corner at 1000 °C (Fig. 7b).

At higher temperatures some information exists for 1200 and 1300 °C (cf. Table 3). Fig. 8 shows a sketch of the isothermal section at 1200 °C based on the available experimental data. These data are from Mazdiyasni et al. [92] for phase equilibria involving τ_3, Kainuma et al. [72] and Tokar et al. [98] for αTi + βTi + TiAl, hitherto unpublished studies by Ducher of αFe/TiAl diffusion couples of ternary Al–Fe–Ti alloys and quinary alloys containing additional amounts of up to 0.5 at.% Nb + Cr, and from Ducher et al. [66] for the compositions of the liquid at the three-phase equilibria. These data are in good agreement with each other and also in accordance with the binary systems except for two points. The tie-triangle reported by Tokar et al. [98] is at variance with the data reported by Kainuma et al. [72] for the same composition range. One possibility for explaining this difference could be the metastable occurrence of τ'_2 in the sample of Tokar et al. as discussed in Section 4. The other point is the observation of the three-phase equilibrium $\tau_3 + TiAl_2 + TiAl_3$ by Mazdiyasni et al. [92]. According to recent investigations of the Al-rich part of the Al–Ti system a single-phase field of 1d-APS/TiAl occurs in the binary Ti–Al system between $TiAl_2$ and $TiAl_3$ at 1200 °C [100], [102] and [108]. Therefore, the three-phase equilibria $\tau_3 + TiAl_2$ + 1d-APS/TiAl and $\tau_3 + TiAl_3$ + 1d-APS/TiAl should be present in the ternary Al–Fe–Ti system at this temperature. This finding is also in full agreement with the reaction scheme in Fig. 4 as are the other tie-triangles that are shown in Fig. 8.

Fig. 8. Sketch of the isothermal section at 1200 °C based on experimental data from Mazdiyasni et al. [92], Kainuma et al. [72], Tokar et al. [98], unpublished studies by Ducher of αFe/TiAl diffusion couples of ternary Al–Fe–Ti alloys and quinary alloys containing additional amounts of up to 0.5 at.% Nb + Cr, and compositions of the melts from Ducher et al. [66]. The dashed tie-triangles show phase equilibria for which no experimental evidence exists right now.

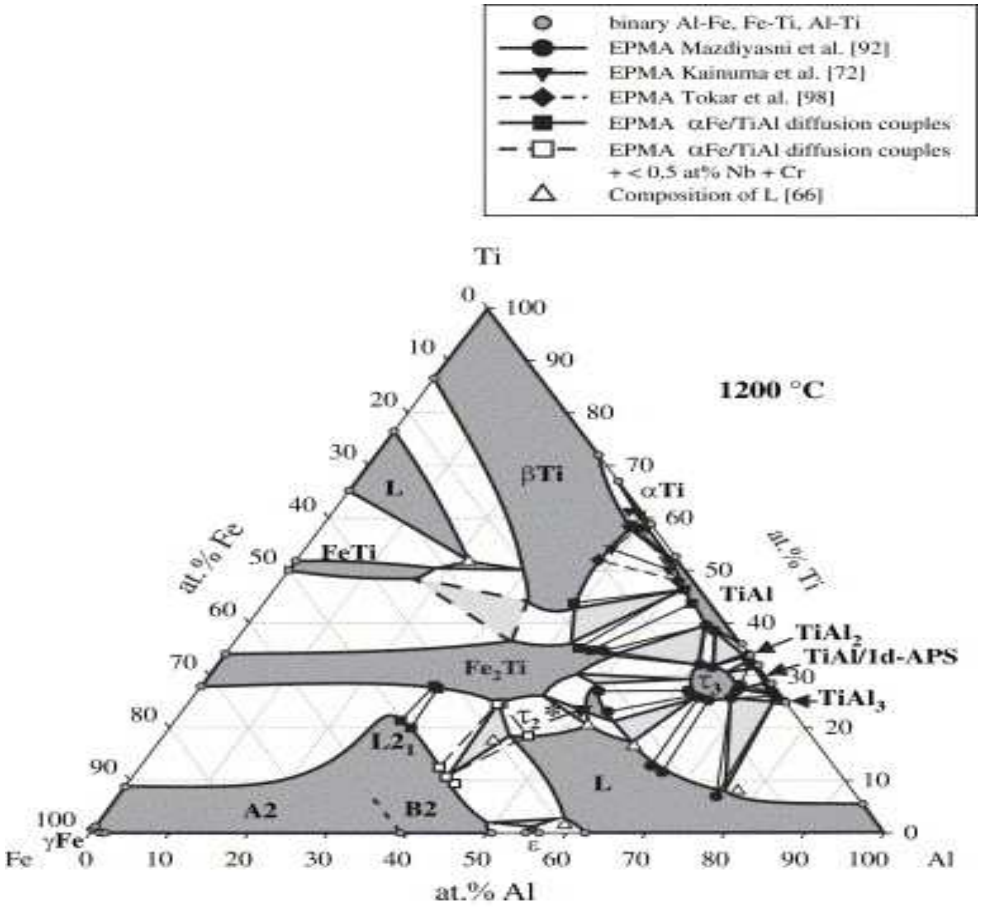

It is noted that also for temperatures below 800 °C some information on phase equilibria exists (cf. Table 3).

8. Magnetic and electrical data

Some magnetic properties of Al–Fe–Ti alloys have been established. Besides the lattice constant, the Curie temperature T_C (123 K) and the saturation moment at 4.2 K have been reported for stoichiometric $L2_1$-ordered Fe_2AlTi aged at 900 °C for 36 h [109]. For $Fe_3Al + x$

Ti (x = 0–11 at.%) the Curie temperature and the magnetization at 77 and 298 K have been determined [81]. Magnetisation and susceptibility measurements in the temperature range 4.2–300 K have also been carried out for $FeAl_{(1-x)}Ti_x$ alloys [88]. Yamada et al. [110] studied the magnetic properties of the C14 Laves phase on alloys $(Fe_{1-x}Al_x)_2Ti$ with $x \leq 0.5$ and found that antiferromagnetism in Fe_2Ti is suppressed by Al substitution and replaced by ferromagnetism. The transition temperature from ferro- to para-magnetism goes through a maximum at about 150 K for x = 0.25.

The electrical resistance has been measured between 600 and 800 °C in order to determine the solid solubility of Fe in αTi [111] and in some Fe_3Al-based alloys [84]. Mössbauer spectra for alloys along $Fe_{3-x}Ti_xAl$ can be found in Refs. [85] and [87].

9. Thermochemical, atomistic and diffusion data

There are few data available for the ternary Al–Fe–Ti system. Bros et al. [112] measured the heat content of various Ti–Al–X alloys, amongst which an alloy with 9.5 at. % Al and 2.1 at. % Fe. They used drop calorimetry up to 600 °C and compared their results with measurements on pure Ti. Thermodynamic properties of alloys of aluminium with iron and titanium have been studied by Gerashchenko and Temnogorova [113].

There are also only few data available on diffusion within the Al–Fe–Ti system. Only recently diffusion data for tracer diffusion of ^{59}Fe within TiAl single crystals [114] and polycrystalline Fe_3Al-based alloys [115] have been reported. Finally, it is worth to mention that stress induced phase transformation in two-phase αTi + βTi alloys has been studied by Koike et al. [116].

10. Modelling

Databases for CALPHAD-type calculations have been made available for each of the corners of the Al–Fe–Ti system. The concerted European COST action 507 has led to the development of a database for aluminium alloys [117] for which assessments were however limited to the description of binary and some ternary systems, but not the Al–Fe–Ti one. In fact, no CALPHAD-type description of the whole ternary Al–Fe–Ti system is available at present. As a matter of fact, the only tentative CALPHAD-type assessment of the Al–Fe–Ti system is due to Dew-Hughes and Kaufman [118] who calculated the 1000 °C isotherm. The extension of both the Laves phase and the B2-ordered phase FeTi in the ternary system was unexpected for these authors, who assumed that Al should have substituted Ti in both phases, and this led them to perform new experiments which just confirmed previous data. Their conclusion, which appears still valid, is that further theoretical studies should attack the problem.

Schön [119] carried out a CVM calculation of the metastable “bcc” Al–Fe–Ti phase diagram, i.e. he calculated the transitions between the A2, B2 and DO_3 structures at 800, 900 and 1000 °C. If only these three phases are considered to be stable, then the B2 structure forms one single-phase field invading a large part of the composition triangle at 1000 °C. The calculations also show that two DO_3 fields exist, one at high Ti content and the other in the Fe-rich corner, which enlarge with decreasing temperature. Emphasis was then put on the various features of the first- and second-order transitions in the Fe-rich corner in comparison with experimental results obtained independently [78].

Ishikawa et al. [120] evaluated the interchange energy between Al and Ti for the next nearest neighbour site when Fe is in the nearest neighbour site in $L2_1$-ordered Fe_2AlTi. They also calculated the phase equilibria between FeAl (B2) and Fe_2AlTi ($L2_1$) in the temperature range 1000–1300 °C and compared them with experimental results. The critical ordering boundary between αTi (disordered A2) and βTi (ordered B2) at 1000 °C has been obtained using the Bragg–Williams–Gorsky approximation [71]. The same method has also been used to calculate the influence of Fe on ordering in $D0_{19}$-type Ti_3Al [121]. Partition coefficients for Fe for phase equilibria involving the phases αTi, βTi, Ti_3Al and TiAl have been evaluated [72]. Details of the kinetics during ordering and disordering in bcc Fe–Al–Ti alloys have been described by use of the micro-master equation method [122]. The phase equilibria in the same composition range have been calculated by use of CVM by Ohnuma et al. [78].

Acknowledgement

This work has been carried out within the frame of COST Action 535, “Thermodynamics of alloyed aluminides (THALU)”.

References

U. Zwicker, J. Breme and K. Nigge, *Mikrochim Acta Suppl* 11 (1985), p. 333.

U. Zwicker, *Z Metallkd* 77 (1986), p. 714.

S. Gärtner and J. Holze, *Aluminium* 65 (1989), p. 1057.

A. Gorzel, M. Palm and G. Sauthoff, *Z Metallkd* 90 (1999), p. 64.

M. Palm, *Intermetallics* 13 (2005), p. 1286.

R.S. Diehm and D.E. Mikkola, *Mater Res Soc Symp Proc* 81 (1987), p. 329.

U. Prakash, K. Muraleedharan, R.A. Buckley, H. Jones and P.A. Shenton, *J Mater Sci* 31 (1996), p. 1569.

Y. Nishino, S. Asano and T. Ogawa, *Mater Sci Eng* A234–A236 (1997), p. 271.

R.S. Sundar, T.R.G. Kutty and D.H. Sastry, *Intermetallics* 8 (2000), p. 427.

S.M. Zhu, K. Sakamoto, M. Tamura and K. Iwasaki, *Scripta Mater* 42 (2000), p. 905.

U. Prakash and G. Sauthoff, *Intermetallics* 9 (2001), p. 107.

S.M. Zhu, K. Sakamoto, M. Tamura and K. Iwasaki, *Mater Trans JIM* 42 (2001), p. 484.

F. Stein, A. Schneider and G. Frommeyer, *Intermetallics* 11 (2003), p. 71.

M. Palm and G. Sauthoff, *Intermetallics* 12 (2004), p. 1345.

H.R. Pak, C.M. Wayman, L.H. Favrow, C.V. Cooper and J.S.L. Pak, *Mater Res Soc Symp Proc* 186 (1991), p. 357.

D.G. Morris and S. Günter, *Acta Metall Mater* 40 (1992), p. 3065.

M.B. Winnicka and R.A. Varin, *Metall Mater Trans* A24 (1993), p. 935.

L. Machon and G. Sauthoff, *Intermetallics* 4 (1996), p. 469. M. Palm, A. Gorzel, D. Letzig and G. Sauthoff In: M.V. Nathal, R. Darolia, C.T. Liu, P.L. Martin, D.B. Miracle and R. Wagner *et al.*, Editors, *Structural intermetallics 1997*, TMS, Warrendale (1997), p. 885.

Ducher R. Contribution à l'étude du diagramme de phase ternaire Fe–Ti–Al et des équilibres Fe–TiAl. Thesis. Toulouse: INP; 2003.

Brady MP, Smialek JL, Brindley WJ. Oxidation-resistant Ti–Al–Fe alloy for diffusion barrier coatings. US Patent no. 5 776 617; 1998.

V. Raghavan, Phase diagrams of ternary iron alloys, part 1, ASM Int, Metals Park (1987) 9.

V. Raghavan, *J Phase Equilib* 14 (1993), p. 618.

V. Raghavan, *J Phase Equilib* 23 (2002), p. 367.

K.S. Kumar, *Int Mater Rev* 36 (1990), p. 293.

G. Ghosh, Aluminium –iron –titanium. In: G. Petzow and G. Effenberg, Editors, *Ternary alloys* vol. 5, VCH, Weinheim (1992), p. 456.

P. Villars, A. Prince and H. Okamoto, *Handbook of ternary alloy phase diagrams* vol. 3, ASM Int, Metals Park (1995) p. 3628.

J.L. Murray, Phase diagrams of binary titanium alloys, ASM, Metals Park (1987) p. 99.

J.L. Murray, Phase diagrams of binary titanium alloys, ASM, Metals Park (1987) p. 12.

H. Okamoto, *J Phase Equilib* 14 (1993), p. 120.

H. Okamoto,*J Phase Equilib* 21 (2000), p. 311.

V. Raghavan, *J Phase Equilib* 26 (2005), p. 171.

Schuster JC, Palm M. J Phase Equilib Diff, accepted for publication.

L. Kaufman and H. Bernstein, Computer calculation of phase diagrams, *Refractory materials* vol. 4, Academic Press, New York (1970) p. 183.

L. Kaufman and H. Nesor In: R.I. Jaffee and H.M. Burte, Editors, *Titanium science and technology* vol. 2, Plenum Press, New York (1973), p. 773.

L. Kaufman and H. Nesor, *Calphad* 2 (1978), p. 325.

J.P. Gros, B. Sundman and I. Ansara, *Calphad* 22 (1988), p. 1587.

J.L. Murray, *Metall Trans* A19 (1988), p. 243.

J.C. Mishurda, J.C. Lin, Y.A. Chang and J.H. Perepezko, *Mater Res Soc Symp Proc* 133 (1989), p. 57.

U.R. Kattner, J.-C. Lin and Y.A. Chang, *Metall Trans* A23 (1992), p. 2081.

M. Oehring, T. Klassen and R. Bormann, *J Mater Res* 8 (1993), p. 2819.

N. Saunders In: I. Ansara, Editor, *COST507: thermochemical database for light metal alloys*, ECSC–EEC–EAEC, Brussels (1995), p. 52.

N. Saunders In: P. Blenkinsop, W.J. Evans and H.M. Flower, Editors, *Titanium '95: science and technology* vol. 3, The Inst. Materials, London (1996), p. 2167.

F. Zhang, S.L. Chen, Y.A. Chang and U.R. Kattner, *Intermetallics* 5 (1997), p. 471.

N. Saunders, COST507: thermochemical database for light metal alloys. In: I. Ansara, Editor, ECSC–EEC–EAEC, Brussels (1995), p. 89.

I. Ohnuma, Y. Fujita, H. Mitsui, K. Ishikawa, R. Kainuma and K. Ishida, *Acta Mater* 48 (2000), p. 3113.

Danilenko VM, Srorchak-Veyduk AN, Yagodkin VV, Bulanova MV, Tretyachenko LA. In: Abstract of the sixth International school-conference phase diagrams in Mater Sci PDMS-VI, Kiev; 2001. p. 233.

U.R. Kattner In: T.B. Massalski, Editor, *Binary alloy phase diagrams* vol. 1, ASM Int, Materials Park (1990), p. 147.

G. Inden and W. Pepperhoff, *Z Metallkd* 81 (1990), p. 770.

O. Ikeda, I. Ohnuma, R. Kainuma and K. Ishida, *Intermetallics* 9 (2001), p. 755.

C. Bichara and G. Inden, *Scripta Metall Mater* 25 (1991), p. 2607.

C.G. Schön, G. Inden and L.T.F. Eleno, *Z Metallkd* 95 (2004), p. 459.

A.O. Mekhrabov, S.I. Masharov, Z.M. Babaev and M.M. Kazymov, *J Turk Phys* 18 (1994), p. 444.

R.K. Bamola and L.L. Seigle, *Metall Trans* A20 (1989), p. 2561.

F. Stein, G. Sauthoff and M. Palm, *Z Metallkd* 96 (2004), p. 469.

A.J. Lendvai, *Mater Sci Lett* 5 (1986), p. 1219.

C.A. Aliravci and Ö Pekgüleryüz, *Calphad* 22 (1998), p. 147.

M. Pashechko and C. Vasyliv, *Z Metallkd* 88 (1997), p. 484.

M. Ellner and J. Mayer, *Scripta Metall Mater* 26 (1992), p. 501.

U. Burkhardt, Y. Grin, M. Ellner and K. Peters, *Acta Crystallogr* B50 (1994), p. 313.

M. Ellner and U. Burkhardt, *J Alloys Compd* 198 (1993), p. 91. C. Freiburg and B. Grushko, *J Alloys Compd* 210 (1994), p. 149.

Burkhardt U, Ellner M, Grin Y, Ipser H, Richter K, Schuster JC, et al. In: Final report international workshop on aluminium – transition metal phase diagrams. Graz, Austria; 1997. p. 54.

M. Palm, *J Alloys Compd* 252 (1997), p. 192.

Eumann M., Phasengleichgewichte und mechanisches Verhalten im ternären Legierungssystem Fe–Al–Mo. Thesis. Aachen: Shaker-Verlag; 2002.

R. Ducher, F. Stein, B. Viguier, M. Palm and J. Lacaze, *Z Metallkd* 94 (2003), p. 396.

M. Palm, G. Inden and N. Thomas, *J Phase Equilib* 16 (1995), p. 209.

V.Y. Markiv, V.V. Burnashova and V.P. Ryabov, Akad Nauk Ukr SSR, *Metallofiz* 46 (1973), p. 103.

L. Levin, A. Tokar, M. Talianker and E. Evangelista, *Intermetallics* 7 (1999), p. 1317.

D. Dew-Hughes, *Metall Trans* A11 (1980), p. 1219.

R. Kainuma, I. Ohnuma, K. Ishikawa and K. Ishida, *Intermetallics* 8 (2000), p. 869.

R. Kainuma, Y. Fujita, H. Mitsui, I. Ohnuma and K. Ishida, *Intermetallics* 8 (2000), p. 855.

Y.L. Hao, R. Yang, Y.Y. Cui and D. Li, *Acta Mater* 48 (2000), p. 1313.

Y.L. Hao, D.S. Xu, Y.Y. Cui, R. Yang and D. Li, *Acta Mater* 47 (1999), p. 1129.

I.M. Anderson, *Acta Mater* 45 (1997), p. 3897.

A.O. Mekhrabov and M.V. Akdeniz, *Acta Mater* 47 (1999), p. 2067.

R. Banerjee, S. Amancherla, S. Banerjee and H.L. Fraser, *Acta Mater* 50 (2002), p. 633.

I. Ohnuma, C.G. Schön, R. Kainuma, G. Inden and K. Ishida, *Acta Mater* 46 (1998), p. 2083.

M.G. Mendiratta, S.K. Ehlers and H.A. Lipsitt, *Metall Trans* A18 (1987), p. 509.

R.T. Fortnum and D.E. Mikkola, *Mater Sci Eng* 91 (1987), p. 223.

C.H. Sellers, T.A. Hyde, T.K. O'Brien and R.N. Wright, *J Phys Chem Solids* 55 (1994), p. 505.

L. Anthony and B. Fultz, *Acta Metall Mater* 43 (1995), p. 3885.

R.N. Wright, J.K. Wright, T.A. Hyde, C.M. Sellers and Y. Mishima In: A.F. Giamei and K. Inoue, Editors, *Mechanical properties and phase transformations of multi-phase intermetallic alloys*, TMS, Warrendale (1995), p. 49.

Y. Nishino, C. Kumada and S. Asano, *Scripta Mater* 36 (1997), p. 461.

G. Athanassiadis, G. Le Caer, J. Foct and L. Rimlinger, *Phys Status Solidi* A40 (1977), p. 425.

Z.Q. Sun, W.Y. Yang, L.Z. Shen, Y.D. Huang, B.S. Zhang and J.L. Yang, *Mater Sci Eng* A258 (1998), p. 69.

K.A. Azez, I.A. Al-Omari, J. Shobaki, M.K. Hasan, G.M. Al-Zoubi and H.H. Hamdeh, *Physica B* 321 (2002), p. 178.

D.E. Okpalugo, J.G. Booth and C.A. Faunce, *J Phys F Met Phys* 15 (1985), p. 681.

T.I. Yanson, N.B. Manyako, O.I. Bodak, R. Cerny, R.E. Gladyshevskii and K. Yvon, *J Alloys Compd* 219 (1995), p. 135.

A. Grytsiv, P. Rogl, G. Giester and V. Pomjakushin, *Intermetallics* 13 (2005), p. 497.

Rogl P, Grytsiv A. Presented at: Workshop Laves phases IV. Düsseldorf; 2005.

S. Mazdiyasni, D.B. Miracle, D.M. Dimiduk, M.G. Mendiratta and P.R. Subramanian, *Scripta Metall* 23 (1989), p. 327.

M. Kogachi, S. Minamigawa and K. Nakahigashi, *Scripta Metall Mater* 27 (1992), p. 407.

M.B. Winnicka and R.A. Varin, *Metall Trans* A23 (1992), p. 2963.

A. Seibold, *Z Metallkd* 72 (1981), p. 712. R. Ducher, B. Viguier and J. Lacaze, *Scripta Mater* 47 (2002), p. 307.

L. Levin, A. Tokar and A. Berner, *J Mater Sci* 35 (2000), p. 3923.

A. Tokar, A. Berner and L. Levin, *Mater Sci Eng* A308 (2001), p. 13.

A. Tokar, L. Levin, A. Katsman, A. Ginzburg, A. Berner and A. Fein *et al.*, *Mater Sci Eng* A351 (2003), p. 56.

M. Palm, L.C. Zhang, F. Stein and G. Sauthoff, *Intermetallics* 10 (2002), p. 523.

S. Hata, K. Shiraishi, M. Itakura, N. Kuwano, T. Nakano and Y. Umakoshi, *J Electron Microsc* 53 (2004), p. 537.

R. Kainuma, J. Sato, I. Ohnuma and K. Ishida, *Intermetallics* 13 (2005), p. 784.

H. Nishimura and E. Matsumoto, *Nippon Kinzoku Gakkaishi* 4 (1940), p. 339.

A. Nwobu, T. Maeda, H.M. Flower and D.R.F. West, User aspects of phase diagrams, Institute of Metals (1991) p. 102.

T.Y. Yang and E. Goo, *Metall Mater Trans* A26 (1995), p. 1029.

M. Palm and G. Inden In: M.V. Nathal, R. Darolia, C.T. Liu, P.L. Martin, D.B. Miracle and R. Wagner *et al.*, Editors, *Structural intermetallics 1997*, TMS, Warrendale (1997), p. 73.

H. Mabuchi, H. Nagayama, H. Tsuda, T. Matsui and K. Morii, *Mater Trans JIM* 41 (2000), p. 733.

J. Braun and M. Ellner, *Metall Mater Trans* A32 (2001), p. 1037.

K.H.J. Buschow and P.G. van Engen, *J Magn Magn Mater* 25 (1981), p. 90.

Y. Yamada, K. Kuroda, A. Sakata and T. Murakami, *J Magn Magn Mater* 177–181 (1998), p. 1397.

L.P. Luzhnikov, V.M. Novikova and A.P. Mareev, *Met Sci Heat Treat* 1963 (1963), p. 78.

H. Bros, M.L. Michel and R. Castanet, *J Therm Anal* 41 (1994), p. 7.

S.L. Gerashchenko and N.V. Temnogorova, Tekhnologiya i oborudovanie proizvodstva tsvetnik i chernik metallov i splavov, Zaporozhye Industrial Institute (1991) p. 4.

N. Terashita, Y. Nose, T. Ikeda, H. Nakajima, H. Inui and M. Yamaguchi, *Mater Lett* 57 (2003), p. 3357.

I.S. Golovin, S.V. Divinski, J. Cizek, I. Prochazka and F. Stein, *Acta Mater* 53 (2005), p. 2581.

J. Koike, Y. Shimoyama, I. Ohnuma, T. Okamura, R. Kainuma and K. Ishida *et al.*, *Acta Mater* 48 (2000), p. 2059.

I. Ansara, A.T. Dinsdale and M.H. Rand, Thermochemical database for light metal alloys, European Commission, Luxembourg (1998).

D. Dew-Hughes and L. Kaufman, *Calphad* 3 (1979), p. 175.

Schön CG. Thermodynamics of multicomponent systems with chemical and magnetic interactions. Thesis. Universität Dortmund; 1998.

K. Ishikawa, R. Kainuma, I. Ohnuma, K. Aoki and K. Ishida, *Acta Mater* 50 (2002), p. 2233.

V.V. Kalyuzhnyi, Z.A. Matysina and M.I. Milyan, *Sov Phys J* 30 (1987), p. 242. J. Ni, T. Ashino and S. Iwata, *Acta Mater* 48 (2000), p. 3193.

Kornilov II, E.N. Pylaeva and M.A. Volkova, *Russ J Inorg Chem* 3 (1958), p. 169.

M.A. Volkova and Kornilov II, *Russ Metall* 1971 (1970), p. 134.

M.A. Volkova and Kornilov II, *Russ Metall* 1971 (1971), p. 137.

R. Kainuma, K. Urushiyama, K. Ishikawa, C.C. Jia, I. Ohnuma and K. Ishida, *Mater Sci Eng* A239–240 (1997), p. 235.

Corresponding author. Tel.: +49 221 6792 226; fax: +49 211 6792 299.